Available online at www.sciencedirect.com
ScienceDirect
Journal of Nuclear Materials 358 (2006) 96–105
journal of nuclear materials
www.elsevier.com/locate/jnucmat

Mixed-material layer formation on graphite exposed to deuterium plasmas containing beryllium

M.J. Baldwin [a,*], R.P. Doerner [a], D. Nishijima [a], K. Schmid [b], D.G. Whyte [c], J.G. Kulpin [c], G. Wright [c]

[a] University of California at San Diego, Center for Energy Research, La Jolla, CA 92093-0417, USA
[b] Max-Planck-Institut für Plasmaphysik, Garching D-85748, Germany
[c] University of Wisconsin, Department of Engineering Physics, Madison, WI 53706, USA

Received 15 March 2006; accepted 13 June 2006

Abstract

Mixed-materials formation and properties are examined for graphite-target surfaces exposed to deuterium plasma containing small amounts of ionized beryllium. Targets are exposed to plasma in the PISCES-B divertor plasma simulator under conditions relevant to the operation of the graphite-strike plates in ITER. X-ray photoelectron spectroscopy (XPS) is used to analyze targets following exposure and reveals chemical reaction of the surface graphite with the incident-plasma beryllium flux. Partial surface carbidization is observed for a target exposure temperature of 450 K and full surface carbidization with Be_2C at temperatures higher than this up to 1000 K. Rutherford backscattering spectrometry (RBS) data reveal a mixed-material layer of Be/C of varying-elemental concentration up to ~1 μm thick. Hydrogen-isotope retention in targets is measured using thermal-desorption spectrometry (TDS) and D-^{3}He nuclear-reaction analysis (NRA). Targets exposed to deuterium plasma exhibit retention consistent with values in the literature but extrapolated to the higher ion fluences possible in PISCES simulators. In contrast, targets with a mixed-material Be/C layer are found to have increased retention by a factor of ~4 at low temperature ~300 K and ~2 at higher temperature ~1000 K. Simulation of NRA spectra reveals that most of the increased inventory is accumulated in the mixed layer.

PACS: 52.40.Hf; 52.77.Dq; 73.50.−h; 73.61.−r

1. Introduction

The international thermonuclear experimental reactor (ITER) design integrates a selection of plasma-facing component (PFC) materials in different locations. For instance, the first wall is to be made from beryllium, the divertor armor from tungsten, and the inclined-strike plates from graphite. Each PFC material is chosen for its specific properties, but in a device like ITER, where erosion by plasma will be ubiquitous, it is unrealistic to expect that each PFC material will be uninfluenced by the other plasma-facing materials. The combination of materials, or 'mixed' materials, can have

* Corresponding author. Tel.: +1 858 534 1655; fax: +1 858 534 7716.
E-mail address: mbaldwin@ferp.ucsd.edu (M.J. Baldwin).

0022-3115/$ - see front matter © 2006 Elsevier B.V. All rights reserved.
doi:10.1016/j.jnucmat.2006.06.014

substantially different properties than specified in the original design, and as such, are a significant concern [1]. Sputtering of the beryllium first wall is indirectly expected to lead to one of the most significant causes of mixed-material formation in the ITER divertor due to bombardment of divertor surfaces with Be ions. The population of Be ions in the divertor plasma is by no means small; the beryllium fraction, $f_{Be} = n_{Be+}/n_e$, defined as the ratio of the density of beryllium ions to electrons, is predicted to be in the range 0.01–0.10 under steady state conditions [2]. Thus, the present experiments focus on the formation of beryllium–carbon mixed materials. Graphite targets are exposed to ITER divertor relevant plasma conditions using the PISCES-B divertor plasma simulator and plasma-beryllium injection system [2], to simulate the kind of material surface effects that may occur on the ITER graphite-strike plates.

Previous PISCES experiments [2–4] identified profound effects on graphite targets exposed to deuterium plasmas containing a beryllium fraction of as little as 0.001, far less than expected in ITER. Net chemical and physical erosion of the target is significantly reduced compared to exposure in pure-deuterium plasma [2,3] and surface analysis, using Auger electron spectroscopy, revealed that the plasma–material interaction (PMI) formed a mixed surface material of composition that depends on f_{Be}, exposure temperature and the plasma fluence [2–5]. While the observations made in these studies are important, the properties of the plasma-induced mixed Be/C material surface were not examined in great detail. This paper probes the mixed-material surface more extensively using a comprehensive collection of surface-diagnostic methods. In particular, surface–chemical interactions between the various mixed-surface elements, mixed-layer composition, and the impact of mixed materials on hydrogen-isotope retention are explored utilizing facilities located at University of California PISCES and the DIONOSIS accelerator facility at the University of Wisconsin-Madison.

2. Experimental procedure

Isostatically molded fine grain graphite 'ATJ' targets, 25 mm in diameter and 2.8 mm thick, are exposed to deuterium plasma containing beryllium in the UC-San Diego PISCES-B facility [2]. In past experiments [2–5], a beryllium fraction, $f_{Be} = 0.001$ is found to produce dramatic changes in the PMI behavior of graphite exposed to deuterium plasma. To facilitate comparison with previous studies, plasma-exposed-graphite targets reported here are subjected to similar plasma conditions: $f_{Be} \sim 0.001$, and $n_e = 3.0 \pm 0.6 \times 10^{18}\ m^{-3}$ and $T_e = 6 \pm 1$ eV as measured with a reciprocating-double probe. A potential bias, V_b of -50 V is applied to targets to achieve low-energy ion bombardment with an estimated ion-impact energy, $e(V_b - V_p) \sim 40$ eV, where the plasma potential, $V_p \sim (V_f + 2kT_e)$ is inferred from measured values of the floating potential, V_f and T_e. Here it is emphasized that this is only the case as the plasma and target sheath are essentially collisionless at the D_2 neutral fill pressures used, $P_N < 1$ Pa. It is pointed out however, that the average energy per impacting D is less than this since there is an ion-species mix in PISCES-B of 53% D^+, 25% D_2^+, and 22% D_3^+, based on the measurements and simulations in [6].

The concentration of ionized beryllium in the plasma is inferred from the intensity of the optical emission from an excited beryllium (Be II) line at 467 nm [2–5]. This measurement relies on a photometric calibration of the optical spectroscopy and viewing optics as well as measurement of n_e and T_e. Plasma parameters are used with the collisional radiative ADAS model [7] to give the resulting beryllium density in the plasma. The reader is referred to Whyte et al. for a detailed description of this procedure [8,9] applied to measuring carbon impurities.

A PHI-surface-analysis system connected to PISCES-B is used to study the surface properties of targets subsequent to plasma bombardment without exposure to atmosphere. The surface-analysis system comprises an Auger electron spectrometer (AES), primarily used for measuring surface composition, and an X-ray photoelectron spectrometer (XPS) that further allows the study of the chemical binding of elements on the target surface. XPS spectra are acquired using a Mg K_α X-ray source and a detector pass energy of 25 eV. The XPS binding-energy calibration is carried out using vacuum-deposited Au and Cu specimens and assigning the Au (4f7/2) and Cu (2p3/2) peaks values of 83.9 eV and 932.5 eV.

Variations in sample-surface morphology and composition are studied using a JEOL-JSM 6830 scanning-electron microscope (SEM) outfitted with INCA energy-dispersive (EDX) and wavelength-dispersive (WDX) X-ray microanalysis systems from OXFORD Instruments.

Information on deuterium inventory and its thermal stability in graphite targets following plasma

exposure is inferred from gas-desorption profiles during thermal-desorption mass spectrometry (TDS) [10]. In TDS, targets are heated linearly in vacuum over 1 h to 1373 K while the partial pressures of deuterium-containing species D_2, HD, D_2O, CD_3 and CD_4 are monitored using a residual-gas analyzer. D_2 and HD are typically prominent desorption species and deuterium retention is calculated from the weighted integral of their partial-pressure profiles. A calibrated-deuterium leak, assumed applicable also for the mixed isotope HD, facilitates conversion of the desorption integrals into a total retention value.

Non-destructive information on the depth location of the beryllium, carbon and deuterium inventory in targets is performed on selected targets using Rutherford backscattering spectrometry (RBS) and nuclear-reaction analysis (NRA). These measurements are conducted using the 1.7 MV Pelletron-tandem-ion accelerator at the University of Wisconsin-Madison. Measurements are made at room temperature using a normally incident 2 MeV $^3He^{2+}$ ion beam with a current ~250 nA as measured by Faraday cup, and with the typical accumulated charge during analysis of 100 μC. A silicon-surface-barrier detector, positioned at a scattering angle of 170°, and subtending a solid angle of 1.1 msr from the beam spot on the surface, is used to measure the energy spectrum of backscattered ^{3}He in RBS, and nuclear-reaction products resulting from ^{3}He incident on D, C and Be in NRA. The beam-spot size is ~5 mm in diameter and centered on the plasma-exposed area of the graphite targets. Data analysis is performed with the SIMNRA numerical simulation code of Mayer [11]. An advantage of ion beam analysis performed at normal incidence is its insensitivity to surface roughness. All depth information is linked to ion slowing at the atomistic scale, thus providing a surface-averaged depth profile of the elements. This is particularly important for the analysis performed here since graphite is difficult to polish and is typically very rough after exposure to plasma.

3. Results

3.1. Electron spectroscopy

In a previous paper [5], it is postulated that the presence of carbide on graphite targets is at least partly responsible for observations of reduced chemical erosion as the mixed Be/C layer evolves. These observations were made for a single target exposure temperature of 700 K. Here we explore further the conditions under which carbide is found to form during plasma exposure by varying the target temperature in the range 450–950 K. Other plasma and target conditions remain consistent. Following exposure, XPS is used to probe the chemical nature of the target surface, as shown in Fig. 1, where photoelectron peaks corresponding to the C 1s and Be 1s core-electron levels are shown. In Fig. 1, exposed target spectra are compared to that of clean-reference samples of metallic beryllium and graphite to facilitate comparison. In all but the lowest temperature case of 450 K, exposed-target surfaces are found to display evidence of chemical reaction with beryllium incident during the exposure. The formation of beryllium carbide is readily observed based on comparison with the reference

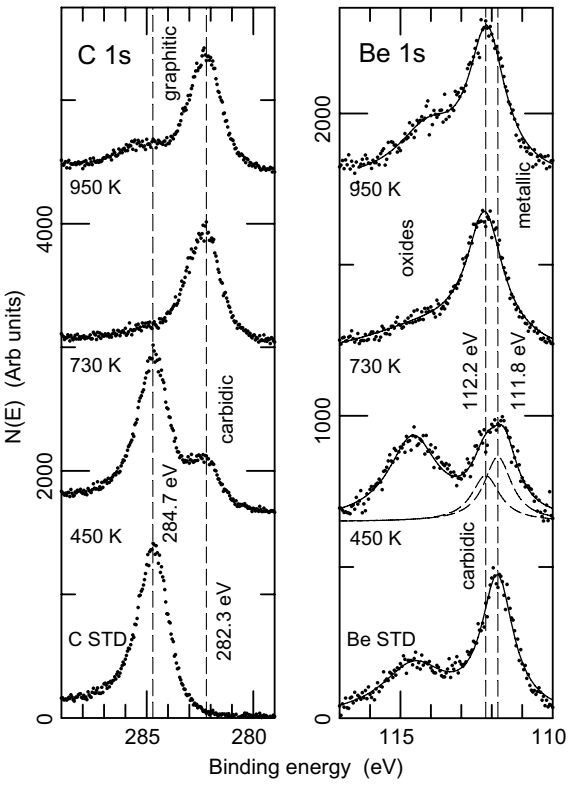

Fig. 1. C 1s and Be 1s X-ray photo-electron spectra taken on graphite targets exposed at 450, 730 and 950 K to deuterium plasma containing beryllium, $f_{Be} = 0.001$. Exposure times were ~3000 s, the plasma density was 1×10^{18} m^{-3} and the electron temperature ~8 eV, respectively. Be 1s spectra for an unexposed clean sample of metallic beryllium is also shown for reference. Dotted lines indicate the binding energies indicative of elemental and carbidic binding.

samples and XPS-peak positions stated in the literature [12,13]. Only the 450 K exposed case shows any sign of elemental graphite and beryllium while targets exposed at higher temperature are found to be fully surface carbidized. Here the graphitic C 1s peak at 284.7 eV is shifted to a carbidic peak at 282.3 eV and the metallic Be 1s peak at 111.8 eV to 112.2 eV.

Electron-microscopy imaging reveals interesting morphology changes in targets exposed to deuterium plasma containing beryllium when compared to targets exposed to pure deuterium plasma. Surface morphology typically varies slightly from exposure to exposure, but generally there are common features that separate graphite targets with and without a mixed Be/C layer. In Fig. 2, an unexposed target is contrast against two targets exposed to plasma at 600 K; one exposed to pure deuterium plasma, the other to deuterium plasma with $f_{Be} \sim 0.001$. On the magnification scale shown, the unexposed target, Fig. 2(a), is very rough and porous in appearance, typical of machined graphite. After exposure to deuterium plasma, Fig. 2(b), the surface develops a 'cone' like appearance typical of the action of chemical erosion at the graphite surface. The target exposed to plasma containing beryllium is remarkably different, Fig. 2(c). With the exception of the observed protrusions, the surface

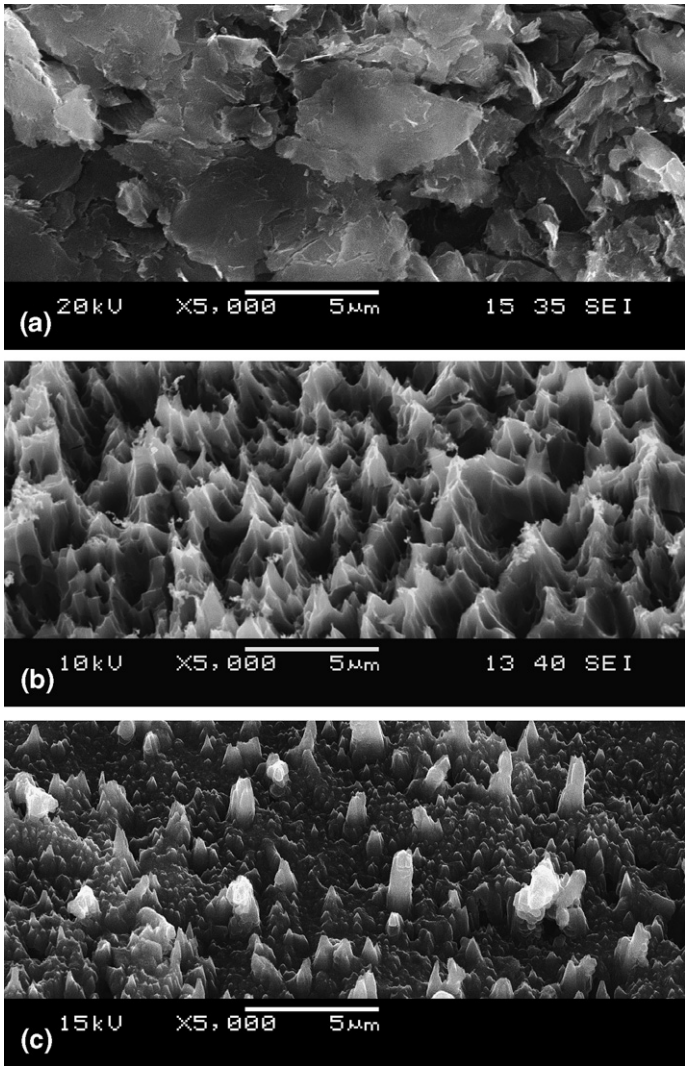

Fig. 2. Electron micrographs of (a) an unexposed graphite target, (b) a deuterium plasma exposed graphite target, D ion fluence $\sim 2.0 \times 10^{26}$ m^{-2} and (c) a target exposed to deuterium plasma with a beryllium fraction $f_{Be} = 0.001$, D ion fluence $\sim 1.2 \times 10^{26}$.

morphology is smoother, typified by a sub-micron level roughness compared to the chemically eroded target. This is presumably due to the deposition of beryllium over the course of the plasma treatment. It is unclear whether the protrusions are left over from net erosion of the surface, or have grown as a result of Be and C deposition/redeposition processes. In either case though, wavelength-dispersive X-ray microanalysis of the protrusions indicates little or no difference in composition (greater than 90 at.% Be) between the protrusions and smoother parts of the target surface. In this regard it is interesting to note that the amount of surface beryllium exceeds that for stoichiometric Be_2C suggesting that a small amount of surface Be is not bound in the carbidic state.

3.2. Ion beam analysis (IBA)

The composition of mixed Be/C layers with depth was studied on two targets using RBS. The backscatter spectra for these targets are shown overlaid in Fig. 3. In RBS spectra, leading edges in a spectrum represent ion-backscatter events from elemental nuclei at the very surface of the target. Projectile ions scattered from deeper within the target surface are measured with lower kinetic energy due to energy loss of the projectile and scattered ion in the material. Fig. 3 contrasts the backscatter spectra for the carbon leading edges of two targets that received different beryllium plasma ion fluences at ~500 K in plasmas where $f_{Be} = 0.0015$. The plasma exposure times are 1600 s and 4600 s, corresponding to beryllium-ion fluences of approximately 3×10^{22} m^{-2} and 1×10^{23} m^{-2}. The spectrum of an unexposed graphite standard (STD) target is also shown for reference.

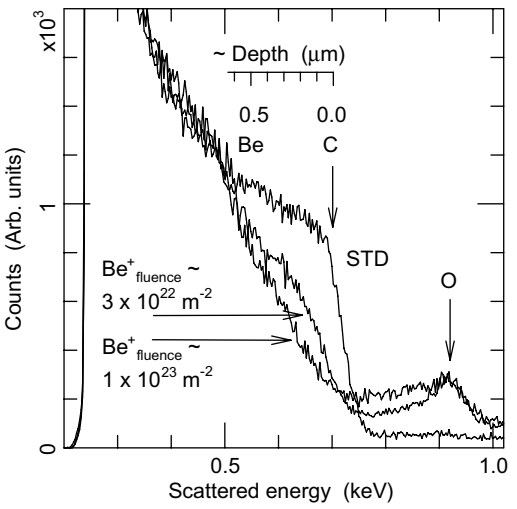

Fig. 3. RBS spectra for 2 MeV $^3He^+$ ions incident on an unexposed reference graphite-target STD, and two graphite targets exposed to deuterium plasmas containing beryllium. The target temperature during plasma exposures was 600 K, $f_{Be} = 0.0015$, and the plasma exposure times, 1600 s and 4600 s corresponding to beryllium ion fluences of approximately 3×10^{22} m^{-2} and 1×10^{23} m^{-2}.

When compared with the unexposed-graphite target, notable count depletion (~0.5–0.7 MeV) is observed on those targets exposed to the plasma containing beryllium, indicating less carbon at the target surface. This is due to the presence of beryllium on these targets as is subsequently confirmed by NRA. The spectra can be simulated [11] with a layer approximately 0.6 μm thick (as indicated schematically), of beryllium concentration gradient varying from ~75 to 85 at.% at the target surface, to ~10–15 at.% at a depth of 0.6 μm. In the simulation, a density of 10^{29} m^{-3} is used for both the layer and underlying graphite and the elastic scattering cross-section for ^3He on C taken from [14]. The feature at $E \sim 0.9$ MeV arises from oxygen in the surface (~10 at.%) and is likely due to exposure of the targets to air before ion-beam analysis. Direct detection of Be (leading edge ~0.5 MeV) is difficult using RBS due to its low-backscatter cross-section. Of particular importance is the thickness of the Be rich layer, which is similar for both targets in spite of the different plasma and Be ion fluences. The target that received a beryllium-ion fluence of 3×10^{22} m^{-2} displays a mixed layer that can account for better than 90% of the incident beryllium during the plasma exposure while the target exposed to the higher fluence of 1×10^{23} m^{-2} has a layer accounting for only about ~30% of the incident beryllium. The similarity in both layers suggests an equilibrium of the target surface composition, at least under the present set of plasma conditions, and is in agreement with earlier results in Ref. [5].

Deuterium concentrations in targets are probed using NRA. Selected spectra for the same targets analyzed with RBS are shown in Fig. 4. Energy spectra for the target exposed to deuterium plasma containing beryllium (Be^+ ~3×10^{22} m^{-2}) is compared to that for a target exposed to pure deuterium plasma and the unexposed standard target (STD). In this figure, features below ~2 MeV are essentially the same as in Fig. 3, but with poorer energy resolution. Beyond 2 MeV, protons produced by ^3He nuclear reactions with Be, C and D lead to

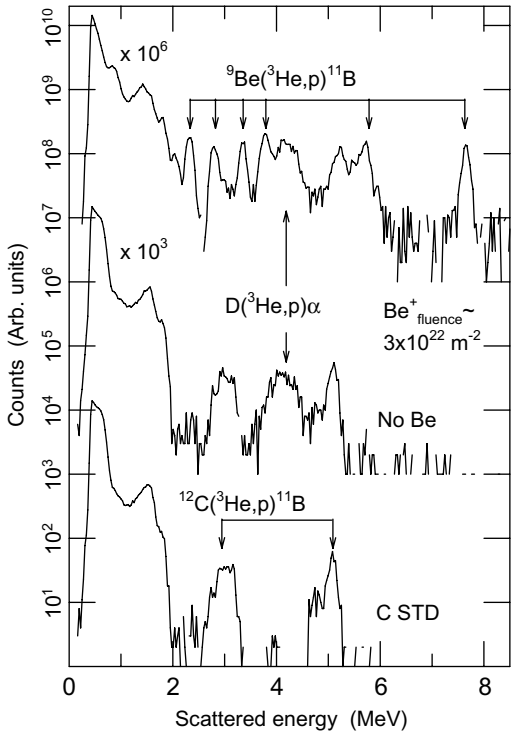

Fig. 4. Compared nuclear-reaction spectra for an unexposed-standard (STD) graphite target, a pure-deuterium plasma-exposed graphite target, and a beryllium-containing ($f_{Be} = 0.0015$, $Be^{+}_{fluence} \sim 3 \times 10^{22}\ m^{-2}$) deuterium-plasma-exposed-graphite target. Measurements are made using a 250 nA, 2 MeV beam of $^{3}He^{2+}$ ions. The scattering angle was 170°.

additional peaks at characteristic energies. Peaks near 3 and 5 MeV (cf. STD spectra) arise from the $^{12}C(^{3}He,p)^{11}B$ reaction [14,15] and are common to each set of spectra. The presence of deuterium leads to a broad peak at ~4 MeV in plasma-exposed targets due to the $D(^{3}He,p)\alpha$ reaction [16]. This peak is expected to appear at only 4 MeV, rather than the actual ~12 MeV for the reaction because of the finite depletion depth of the Si detector and was properly taken into account in the analysis. A stopping foil was not used in order to simultaneously measure all of the NRA peaks. Based on the range of 2 MeV ^{3}He in C, this technique is sensitive to D up to ~5 μm. For the target exposed to plasma containing beryllium, additional peaks arise from $^{9}Be(^{3}He,p)^{14}N$ [17] reactions with surface beryllium. SIMNRA [11] is also used to simulate the spectra in Fig. 4 in order to obtain information about the location of deuterium in the target-surface region. The simplest approach is to model the nuclear stopping range with a specific number of compositionally homogeneous layers to achieve a good fit to the nuclear spectra. These layers are specified as an areal density in atoms/m^2. Translation to depth requires knowledge of the density of the material, which can be affected by porosity, swelling due to disorder, damage and the inclusion of deuterium. However, for reference purposes, an areal density of $\sim 10^{20}$ atoms/m^2 in graphite corresponds to approximately 1 nm. In Fig. 4, the target exposed to pure deuterium plasma shows spectral features that are best simulated using a constant D/C ratio of 0.01 through a surface layer of areal density $1.6x10^{23}\ m^{-2}$ (~1.6 μm), resulting in a D retention of $\sim 1.6 \times 10^{21}\ m^{-2}$. For the targets exposed to beryllium containing plasma, the D/(Be + C) ratio is ~0.03–0.07 in a surface layer of areal density $\sim 1.1 \times 10^{23}\ m^{-2}$ (~1.1 μm), leading to total retention values of $3.3 \times 10^{21}\ m^{-2}$ and $7.1 \times 10^{21}\ m^{-2}$ for the beryllium fluence cases of $1 \times 10^{23}\ m^{-2}$ and $3 \times 10^{22}\ m^{-2}$. That is, in targets exposed to beryllium during exposure, D retention is approximately 2–4 times larger on comparison to the corresponding case without beryllium, and the deuterium is located over a more shallow depth, predominately in the mixed Be/C layer. The depth location of the trapped deuterium is made less uncertain by reducing the beam energy to 550 keV, which reduces the sensitivity of the technique to approximately the first 1 μm below the surface due to the reduced range of ^{3}He in the C/Be layer. The results for this lower beam energy agree well with the 2 MeV NRA results indicating that retained deuterium is largely concentrated in the first ~1 μm. According to the RBS data of Fig. 3, the first ~1 μm is almost entirely mixed Be/C layer.

3.3. Thermal-desorption mass spectrometry

The influence of beryllium on deuterium retention is explored further using TDS. Fig. 5 shows desorption spectra for two target temperature regimes of ~600 K and ~1000 K. Spectra for targets exposed to pure deuterium plasma and deuterium plasma with $f_{Be} = 0.001$ are compared. Targets exposed to pure deuterium plasma received a total ion fluence of $4.0 \times 10^{26}\ m^{-2}$ while those subject to plasma containing beryllium received a smaller fluence of only $2.0 \times 10^{26}\ m^{-2}$.

Fig. 5 shows desorption flux trends for the deuterium containing species, $m/e = 3$ (HD), 4 (D_2) as the targets are heated under vacuum at 0.3 K s^{-1} to 1373 K. There is no convincing trend in CD_4 desorption, nor are any other deuterium species found to

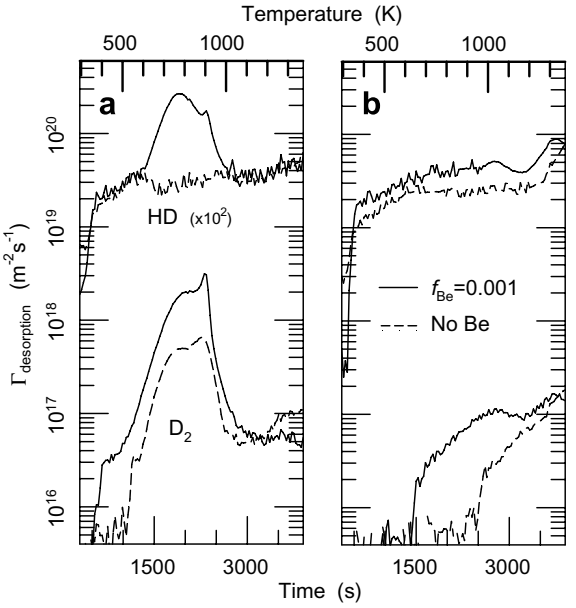

Fig. 5. Thermal-desorption-spectrometry profiles for graphite targets exposed to pure deuterium and deuterium with beryllium ($f_{Be} = 0.001$) plasma at ~600 and 1000 K. The deuterium ion fluence was $4.0 \times 10^{26}\,m^{-2}$ for the case without beryllium injection and $2.0 \times 10^{26}\,m^{-2}$ for the cases with beryllium injection.

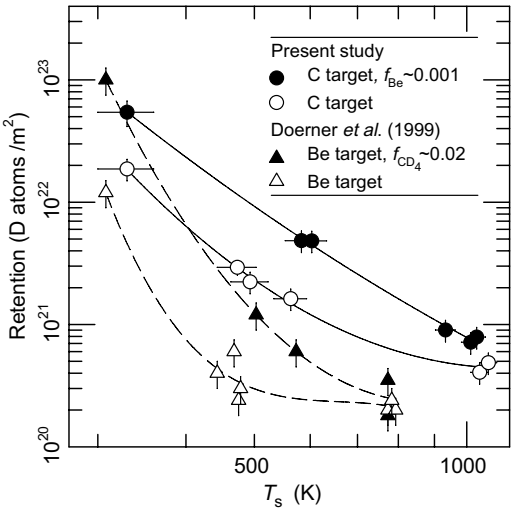

Fig. 6. Deuterium retention in targets as a function of target temperature during plasma exposure. Data are shown for the present study, graphite targets exposed to deuterium plasma with and without beryllium injection ($f_{Be} = 0.001$) and compared to data from Doerner et al. [18], pure beryllium targets exposed under similar plasma conditions with and without deuterated methane (CD_4, ~2%) injection. Both data sets reveal increased retention where a mixed beryllium/carbon surface is present.

have significant release trends. As with the NRA results, the deuterium uptake in graphite is increased in targets exposed to plasma containing beryllium compared to plasma without beryllium. For targets exposed ~600 K, thermal release is characterized by a release peak ~800 K with better than a factor of 4 increase in the amount of desorbed deuterium in the mixed-material case. The targets exposed at ~1000 K do not show strong thermal release ~800 K presumably because of the higher temperature during plasma exposure. In both temperature regimes the mixed-material surface shows a reduced temperature for the onset of desorption.

In Fig. 6, deuterium retention is plotted against target-surface temperature during exposure. Data are shown for graphite targets exposed to both pure, and beryllium containing, $f_{Be} = 0.001$, deuterium plasma exposures. The plasma fluences vary from $2–5 \times 10^{26}$ D ions m^{-2} in this data set. The plot shows that retention falls significantly with exposure temperature; a result, in pure graphite, that has also been observed by others [29]. In contrast, targets with a mixed Be/C material surface show systematically higher retention than targets without. Retention in targets with a mixed-material surface is increased by ~4 at temperatures below 600 K but this difference is reduced to ~2 at ~1000 K. Interestingly, similar trends are observed in the reversed scenario. Also shown in Fig. 6 are PISCES mixed-materials retention data from Doerner et al. [18]. In those experiments, pure-beryllium targets are exposed under similar conditions to the present study, and retention is compared for plasma exposures with and without deuterated methane (CD_4, ~2%) injection. As with the present study, retention is increased in beryllium targets with a mixed-material layer and the difference narrows at temperatures beyond 600 K.

4. Discussion

The erosion of carbon-based materials by particle impact has long been a concern in fusion experiments. The actions of chemical and physical sputtering represent significant material-loss mechanisms contributing not only to reduced carbon PFC lifetime but also impurity buildup in the plasma and carbon film deposition at other vessel locations. With reference to ITER, the additional bombardment of the graphite-strike plates with beryllium originally sputtered from the first wall, further complicates these issues and concerns. In previous PISCES-simulator experiments [2–5], it is shown

that graphite targets under exposure to deuterium plasma are more resilient to the effects of chemical and physical erosion when an ionized-beryllium concentration is present in the plasma. This reduction in erosion is observed to coincide with the presence of beryllium on the target surface. At even moderate-target temperatures as low as 450 K, the data of Fig. 1 reveal that surface beryllium chemically binds with the graphite under divertor simulator conditions and this process is more efficient as target temperature is increased. At higher temperature, surface–chemical reaction leads to fully-surface-carbidized targets that exhibit XPS binding-energy shifts in Be 1s and C 1s electron levels consistent with the formation of Be_2C [12]. Similar reactions and behavior with temperature have also been observed in the phase-formation studies of Linsmeier et al. [13] and Roth et al. [19] where carbon films evaporated onto a beryllium substrate show progressive carbide conversion with increased thermal-anneal temperature. Other than these, there are several laboratory studies reported in the literature in which the chemical interaction of beryllium and carbon is examined. Beryllium carbide formation is observed on beryllium substrates exposed to plasma with carbon impurities [20], in plasma-assisted deposition experiments [21], and on beryllium targets in e-beam evaporative deposition [12,13] experiments. It is therefore not too surprising that beryllium carbide is found to occur in the present experiments under the reverse scenario where graphite targets are exposed to plasma with an incident-beryllium flux.

The presence of beryllium carbide in the mixed-material surface is almost certain to contribute to observations [2–5,18] of target resilience to plasma erosion. Both experimental [22] and TRIMSP calculations [23] reveal sputter yields for beryllium in Be_2C that are significantly less than the yield for pure beryllium, which means that bound-carbidic beryllium is comparably more difficult to remove than unbound beryllium. While the yield for C in Be_2C is slightly increased (compared to pure C/graphite) due to differences in the surface binding energies for beryllium and carbon [22], the resultant preferential erosion of surface C only serves to increase the concentration of beryllium on the target surface, thus contributing to a shielding effect. This is somewhat suggested by the observation of target-surface-beryllium concentrations larger than that corresponding to the stoichiometry of Be_2C, as is described in Sections 3.1 and 3.2.

Direct shielding of the underlying graphite from the plasma offers a simple explanation for reduced target erosion and is also observed in the experiments of others. In the ion beam experiments of Balden [24–26] and co-workers, fine-grain and atomically-dispersed-carbide-doped graphites are found to show a monotonic reduction in chemical erosion by hydrogen ions when compared to undoped specimens. Geometrical shielding of the underlying graphite is believed to be responsible as progressive surface enrichment with the dopant metal carbide is caused by preferential erosion of carbon in the target matrix. However, other evidence in the literature would suggest that carbides could play a more fundamental role in reducing chemical erosion. Reduced activation for hydrogen release and differing temperature dependencies for CD_3 and CD_4 in metal-carbide-doped graphites [24–26], reveal differences in the chemical-erosion mechanism where carbide is present. Observed morphology differences on beryllium-exposed targets, as in Fig. 2, are visible evidence that beryllium acts to geometrically shield the underlying target from plasma erosion. A beryllium-rich more uniform surface is evident, that, as a separate issue, may also be less prone to the effects of dust production owing to less complex surface features.

With reference to the RBS plots of Fig. 3, it is worth noting that a thick layer of deposited pure beryllium over the $\sim$0.6 μm thick mixed-material layer is not observed despite the factor of $\sim$3 difference in deposited-beryllium fluence. This would suggest, at least for the conditions of the current experiment, that once a lower sputter yield carbide layer forms, subsequently deposited beryllium in an overlayer is readily re-eroded because of its higher sputter yield [22], thus producing an equilibrium condition for the Be/C layer depth. Therefore it also important to realize that the redeposition fraction of re-eroded Be, which will be much higher in the high density ITER divertor, will play an important role in the equilibrium Be/C film depth in a given situation.

Retention measurements made using IBA and TDS techniques show that a mixed-material Be/C layer significantly increases hydrogen-isotope trapping. NRA measurements show that the deuterium is trapped at shallow depths with most of the deuterium located in the mixed-material surface. However, in spite of this, TDS thermal release characteristics, as in Fig. 5, show remarkable similarity suggesting that the release mechanisms are tied with

carbon rather than beryllium carbide or beryllium. In this regard it is further noted that desorption trends in Fig. 5 are not reminiscent of pure beryllium [27] or beryllium codeposits [28] but some similarity is evident on comparison with TDS studies of doped graphites [29]. In [29], D_3^+ ion-implanted doped graphites show a similar reduced onset temperature for D_2 release and similar desorption profiles compared to undoped specimens. A further comparison can be made for the graphite targets of this study that are exposed to pure deuterium plasma; deuterium retention values and dependence on exposure temperature are also found to be consistent with data reported in [29]. However, the presence of a mixed Be/C layer on targets increases deuterium retention significantly, up to a factor of 4 at low temperature ~300 K, but less at ~2 at temperatures ~1000 K. While differences prevent any meaningful comparison, it is worthwhile noting that such trends are at least consistent with retention studies on carbide-doped graphites [30] in spite of the chemical and structural differences between the carbidic layers of this study and the doped graphites of Ref. [30].

In considering how the results of this study relate to an ITER scenario it is possible to speculate that at least parts of the surface of the ITER graphite-strike plates may be dominated by carbidic reactions with the incident-beryllium flux, and that hydrogen-isotope retention may be increased compared to pure graphite. While the strike points are expected to operate above 1300 K [31], much higher than examined in this study, the strike plate is exposed to a steep heat-flux profile and cooler regions of the graphite might be prone to the effects observed in the temperature range <1000 K of this study. However, there are further differences between tokamacs and plasma simulators that nevertheless prevent a direct comparison. Influences due to ion-impact geometry and energy distribution, and divertor asymmetries and torroidal flows for instance, can only really be examined in an actual torroidal device.

A further question is whether or not Be/C mixed-material layers will survive in the ITER environment. Edge localized modes (ELMs), expected at frequency of ~1 Hz, are expected to be a dynamic cause of surface particle removal in ITER, which may be sufficient to remove the mixed-material layer. In simulator experiments [32], Federici et al. have studied the removal of aluminum (used to emulate beryllium) from graphite under ITER relevant heat loads and find that the metal layer does not deteriorate until the metal surface layer reaches the Al boiling point. It is unclear if the same behavior will occur for a beryllium layer since carbidic binding may inhibit the boiling action. Recent modifications to PISCES-B, which allow target-heat pulsing in addition to continuous beryllium-containing plasma operation, are to be used to examine such phenomena in the near future.

5. Summary

In summary, the interaction of the ITER graphite-strike points with divertor plasma containing beryllium is simulated in the divertor-plasma-simulator PISCES-B. Surface chemical reaction with the incident-beryllium flux is found to dominate graphite-target PMI above 450 K, forming a thin mixed-material Be/C layer ~1 μm thick with full or partial Be_2C carbide fractions. Targets with a mixed-material Be/C layer are found to have increased retention in the exposure temperature range 300–1000 K. Retention is greater by a factor of ~4 at low temperature ~300 K and ~2 at higher temperature ~1000 K. Analysis of selected targets using NRA reveals that most of the increased inventory is accumulated in the mixed layer.

Acknowledgements

The authors gladly wish to acknowledge the skill and dedication displayed by technical staff associated with the maintenance and operation of the PISCES-B facility. This work is conducted under the US Department of Energy under Contract: DOE DE-FG03-95ER-54301.

References

[1] G. Federici, P. Andrew, P. Barabaschi, J. Brooks, R. Doerner, A. Geier, A. Herrmann, G. Janeschitz, K. Krieger, A. Kukushkin, A. Loarte, R. Neu, G. Saibene, M. Shimada, G. Strohmayer, M. Sugihara, J. Nucl. Mater. 313–316 (2003) 11.
[2] R. Doerner, M.J. Baldwin, K. Schmid, Phys. Scripta T111 (2004) 75.
[3] K. Schmid, M.J. Baldwin, R. Doerner, A. Wilthner, Nucl. Fusion 44 (2004) 815.
[4] K. Schmid, M. Baldwin, R. Deorner, J. Appl. Phys. 97 (2005).
[5] M.J. Baldwin, R.P. Doerner, Nucl. Fusion 46 (2006) 444.
[6] E.M. Hollmann, G. Antar, R.P. Doerner, S.C. Luckhardt, Rev. Sci. Instrum. 72 (1) (2001) 623.
[7] H.P. Summers, Atomic Data and Analysis Structure – User Manual, Report No. JET-IR(94), 1994.

[8] D.G. Whyte, R.P. Seraydarian, R.P. Doerner, J. Vac. Sci. Technol. A 17 (1999) 2713.
[9] D.G. Whyte, G.R. Tynan, R.P. Doerner, J.N. Brooks, Nucl. Fusion 41 (1) (2001) 47.
[10] M.H. Mintz, I. Jacob, D. Shaltiel, in: L. Schlapbach (Ed.), Topics in Applied Physics, Hydrogen in Intermetallic Compounds II, vol. 67, Springer, New York, 1988.
[11] M. Mayer, SIMNRA User's Guide, Report IPP 9/113, Max-Planck-Institut fur Plasmaphysik, Garching, Germany, 1997.
[12] P. Goldstrass, K.U. Klages, Ch. Linsmeier, J. Nucl. Mater. 290–293 (2001) 76.
[13] Ch. Linsmeier, J. Luthin, P. Goldstraß, J. Nucl. Mater. 290–293 (2001) 25.
[14] H. Kuan, T.W. Bonner, J.R. Risser, Nucl. Phys. 51 (1964) 481.
[15] D.A. Bromley, E. Almqvist, H.E. Gove, A.E. Litherland, E.B. Paul, A.J. Ferguson, Phys. Rev. 105 (1957) 957.
[16] H.S. Bosch, G.M. Hale, Nucl. Fusion 32 (1992) 611.
[17] E.A. Wolicki, H.D. Holmgren, R.L. Johnston, E. Geer Illsley, Phys. Rev. 116 (1959) 1585.
[18] R.P. Doerner, A.A. Grossman, S. Luckhardt, R. Seraydarian, F.C. Sze, D.G. Whyte, J. Nucl. Mater. 266–269 (1999) 392.
[19] J. Roth, W.R. Wampler, W. Jacob, J. Nucl. Mater. 250 (1997) 23.
[20] J. Won, F.E. Spada, R. Boivon, R. Doerner, S. Luckhardt, F.C. Sze, R.W. Conn, J. Nucl. Mater. 241–243 (1997) 1110.
[21] Y. Xie, N.C. Morosoff, W.J. James, J. Nucl. Mater. 289 (2001) 48.
[22] E. Gauthier, W. Eckstein, J. László, J. Roth, J. Nucl. Mater. 176–177 (1990) 438.
[23] J.N. Brooks, Argonne National Laboratories, personal communication, 2005.
[24] M. Balden, C. García-Rosales, R. Behrisch, J. Roth, P. Paz, J. Etxeberria, J. Nucl. Mater. 290–293 (2001) 52.
[25] C. García-Rosales, M. Balden, J. Nucl. Mater. 290–293 (2001) 173.
[26] M. Balden, J. Roth, E. de Juan Pardo, A. Wiltner, J. Nucl. Mater. 231–316 (2003) 348.
[27] R.P. Doerner, R.W. Conn, S.C. Luckhardt, F.C. Sze, J. Won, Fusion Eng. Des. 49–50 (2000) 183.
[28] M.J. Baldwin, K. Schmid, R.P. Doerner, A. Wiltner, R. Seraydarian, Ch. Linsmeier, J. Nucl. Mater. 337–339 (2005) 590.
[29] A. Haasz, J. Davis, J. Nucl. Mater. 232 (1996) 219.
[30] M. Mayer, M. Balden, R. Behrisch, J. Nucl. Mater. 252 (1998) 55.
[31] G. Federici, R.A. Anderl, P. Andrew, J.N. Brooks, R.A. Causey, J.P. Coad, D. Cowgill, R.P. Doerner, A.A. Haasz, G. Jneschitz, W. Jacob, G.R. Longhurst, R. Nygren, A. Peacock, M.A. Pick, V. Philipps, J. Roth, C.H. Skinner, W.R. Wampler, J. Nucl. Mater. 266–269 (1999) 14.
[32] G. Federici, A. Zhitlukhin, N. Arkhipov, R. Giniyatulin, N. Klimov, I. Landman, V. Podkovyrov, V. Safronov, A. Loarte, M. Merola, J. Nucl. Mater. 337–339 (2005) 684.